JOURNAL OF SOLID STATE CHEMISTRY **132,** 113–122 (1997)
ARTICLE NO. SC977418

Cation Ordering in [(Tl, *M*)O] Layers of "1201"-Based Cuprates: Similarity to Ordering in fcc-Based Alloys

G. Van Tendeloo,* P. De Meulenaere,* F. Letouzé,† C. Martin,† M. Hervieu,† and B. Raveau†

*EMAT, University of Antwerp (RUCA), Groenenborgerlaan 171, B-2020 Antwerp, Belgium; and †CRISMAT, ISMRA, Université de Caen, Boulevard Maréchal Juin, 14150 Caen Cedex, France

Received December 23, 1996; in revised form April 8, 1997; accepted April 9, 1997

"1201" Tl-based substituted cuprates of the type $(Tl_{1-x}M_x)Sr_2CuO_5$ have been synthesized for M = Nb, Ta, or W. These materials do not superconduct due to a statistical distribution of some of the M for Cu. The remarkable feature of these materials is the ordering observed between Tl and M in the $(Tl_{1-x}M_{x-\varepsilon})O$ plane. The type of ordering depends on the composition and shows remarkable similarities with the ordering in Ni–Mo or other so-called 1 1/2 0 type fcc-based alloys or with the ordering in rocksalt oxides TiO_x. The short-range order, for M = W, can be readily interpreted in terms of a mixing of nano-clusters with two different compositions. These observations of two-dimensional ordering confirm recent ideas about ordering in three-dimensional fcc-based alloys.

1. INTRODUCTION

The studies during recent years on mercury-based cuprates have shown that the substitution of transition metal elements for mercury allows large series of superconductors with generic formulas $(Hg,M)S_2Ca_{m-1}Cu_mO_{2m+2+x}$ (1–4) or $(Hg,M)Ba_2Ca_{m-1}Cu_mO_{2m+2+x}$ (5–8) to be generated. However, very few thallium cuprates, involving the presence of a transition element on the Tl sites, have been synthesized up to now. The doping of the nonsuperconducting $TlSr_2CuO_{5-x}$ phase (9–16) with Cr led to the discovery of a superconductor with $T_c = 40$ K (17). The latter is actually an oxychromate, involving an ordered distribution of Tl cations and chromate groups according to the formula $Tl_3(CrO_4)Sr_8Cu_4O_{16}$ (18). Recently Mo was substituted for Tl in $TlSr_2CuO_{5-x}$ (11); this phase however is nonsuperconducting.

The above results suggest that it should be possible to substitute other transition elements for thallium and to gain an understanding of the influence of such substitutions upon the possible appearance of superconductivity.

In the present contribution we report not only the presence of new "1201"-type Tl cuprates of the type $Tl_{1-x}Sr_2Cu_{1-y}M_{x+y}O_{5-\delta}$ with M = Ta, Nb, or W, but we also determine the remarkable ordering of M within the Tl–O plane and relate it to ordering in fcc-based alloys of the Ni_4Mo type.

2. EXPERIMENTAL CONDITIONS

The samples were prepared starting from mixtures of Tl_2O_3, SrO_2, Sr_2CuO_3, CuO, and Nb_2O_5 or Ta_2O_5 or WO_3, weighted in stoichiometric proportions, according to the general formula $Tl_{1-x}M_{x+y}Sr_2Cu_{1-y}O_5$, with M = Nb, Ta, or W; $0 < y < 0.3$ and $0 < x < 0.2$. The mixtures were homogenized by grinding in an agate mortar, pressed in the form of bars, and sealed in evacuated silica tubes. The ampoules were directly introduced into a hot furnace at 880°C, maintained for 12 hr at this temperature, and then quenched to room temperature.

The powder X-ray diffraction patterns were registered by step scanning over an angular range of $10^\circ \le 2\theta \le 80^\circ$ with an increment of 0.02° (2θ), with a Philips diffractometer using Cu$K\alpha$ radiation. Structure calculations were carried out, using the Rietveld method (19) (Program Fullprof (20)).

Samples for electron microscopy are obtained by crushing the material in alcohol or in *n*-butanol and dispersing the flakes on a holey carbon copper or nickel grid. A major difficulty was the strong anisotropy of most of the samples; the overwhelming majority of the samples was oriented with the [001] axis more or less parallel to the electron beam. The electron diffraction (ED) study was carried out with a JEOL 200CX electron microscope fitted with a tilting rotating sample holder ($\pm 60^\circ$). High resolution electron microscopy (HREM) was performed with a TOPCON 002B or a Jeol 4000EX electron microscope, having a point resolution of 1.8 Å. Both microscopes are fitted with Kevex analyzers for energy dispersive spectrometry (EDS). Image calculations are performed using the Mactempas program.

3. RESULTS

X-ray diffraction confirms the formation of the 1201-type structure for all transition elements M mentioned; evidence

0022-4596/97 $25.00

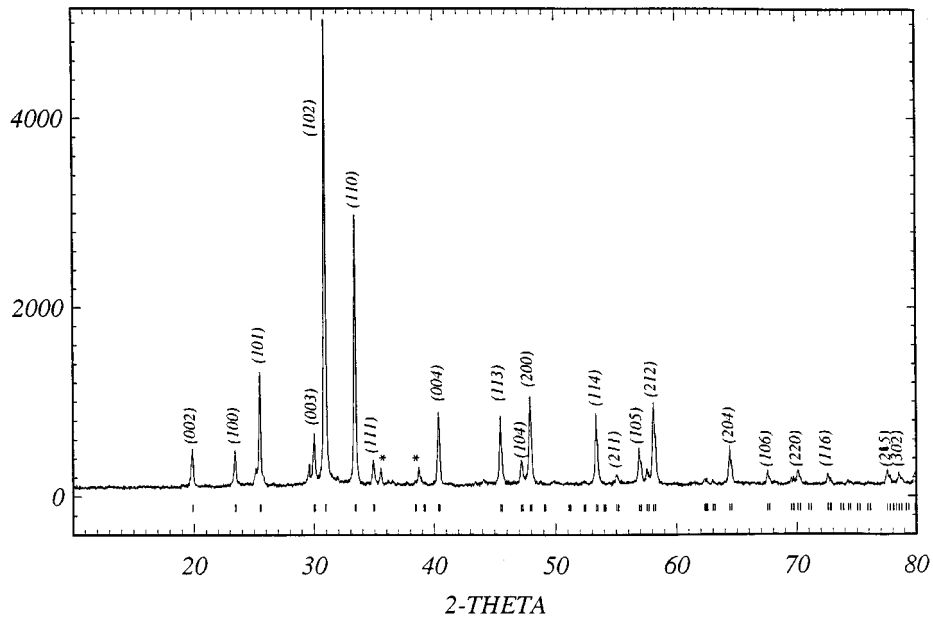

FIG. 1. X-ray spectrum of a sample with nominal composition $Tl_{0.8}W_{0.2}Sr_2CuO_5$; the material is almost single phase with only a small impurity content (CuO, indicated by *) and all reflections can be indexed based on a 1201-type cell, such as the one in Fig. 2.

is shown in Fig. 1 for the W-substituted cuprate with nominal composition $Tl_{0.8}W_{0.2}Sr_2CuO_5$. The full structure analysis was carried out by a combination of XRD, EDS, ED, and HREM. The two latter techniques provide strong evidence for supplementry ordering in the Tl-plane, which cannot be detected by XRD. A schematic representation of the 1201-type structure with the indication of the possible ordering is given in Fig. 2.

We first present the XRD and EDS results since they describe the average structure; then we deduce the local structure by electron diffraction and HREM.

3.1. The Average Structure: X-Ray Analysis and EDS

The EDS analyses are systematically performed on numerous crystallites, for every sample. They show that the sample compositions are rather homogeneous. The results show common behavior for the three compounds: a deficiency of copper as well as of thallium. The measured average sample compositions are given in Table 1. The formulas are calculated based on a full occupancy of the strontium sites, i.e., 2 per formula unit. For the W sample, the copper content is close to 1 and the W content is ≈ 0.2 while for the Nb and Ta samples, the copper content is lower (≈ 0.8) but the M content is higher (≈ 0.3). These results suggest that the transition elements are located on both the Tl and the Cu positions, particularly for Nb- and Ta-based samples. This behavior is different from the results observed for M = Mo (11) (Mo is only substituting for Tl), as well as from the results in Cr-based compounds which form chromate groups exhibiting long-range ordering with the thallium polyhedra, similar to those observed in the carbonate groups in the 1201 phases (see (21) for a review). It should be noted that there is always a small cation deficiency since $M + Tl \approx 0.9$, but this is not unusual for thallium-based layered cuprates.

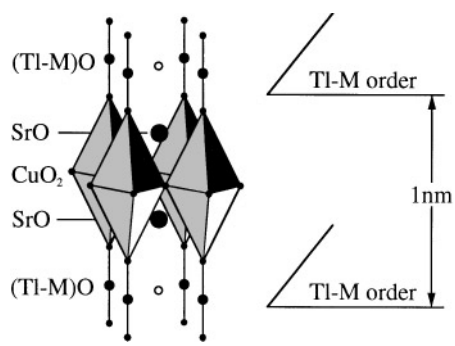

FIG. 2. Schematic representation of the "1201" type structure of $TlSr_2CuO_5$.

TABLE 1
Cell Parameters and Cationic Compositions

Ideal composition	Actual composition	a (Å)	c(Å)
$Tl_{0.8}Nb_{0.2}Sr_2CuO_z$	$(Tl_{0.85}Nb_{0.15})Sr_2(Cu_{0.8}Nb_{0.2})$	3.7942(2)	8.9310(5)
$Tl_{0.8}Ta_{0.2}Sr_2CuO_z$	$(Tl_{0.8}Ta_{0.1})Sr_2(Cu_{0.8}Ta_{0.2})$	3.7925(2)	8.9443(5)
$Tl_{0.8}W_{0.2}Sr_2CuO_z$	$(Tl_{0.75}W_{0.15})Sr_2(Cu_{0.95}W_{0.05})$	3.7745(2)	8.9505(4)
$TlSr_2CuO_z$		3.7344(5)	9.007(1)

The cell parameters of the different phases (see Table 1) are significantly different from those of the nonsubstituted 1201 phase $TlSr_2CuO_{5-\delta}$ (9). The a parameters increase whereas the c parameters decrease; the effect is maximum for Nb and Ta, suggesting that the evolution is strongly correlated to the copper substitution. For the X-ray study, new compounds have been prepared according to the composition determined by EDS in order to avoid inhomogeneities and the presence of secondary phases.

XRD refinements are carried out in the average cell with the space group $P4/mmm$; the starting atom positions were those usually considered for a Sr-based 1201 cuprate. The positional parameters, occupancy factors, and thermal factors of the cations were first refined; the positional parameters of the oxygen were refined in a second step, keeping their B factors constant in 1 $Å^2$.

One observes an excess of electrons on the copper sites and a deficiency on the thallium sites. Within the limit of accuracy of the refinement of such complex structure by powder XRD patterns, the mixed occupancy of the two types of sites is consistent with the EDS analyses and the cation distribution displayed in Table 1. However, the R factors are close to 0.1 and cannot be lowered; this can be understood by the Tl–M ordering observed by electron microscopy.

3.2. The Local Structure: ED and HREM

Electron diffraction patterns along several zone axes confirm the "1201" basic structure with tetragonal lattice parameters $a_{1201} \approx a_p$ and $c_{1201} \approx 9$ Å. Evidence is provided in Figs. 3a and 3b; no extinction conditions are observed, compatible with the P-type symmetry.

For the samples with M = Ta, Nb, or W, well pronounced ordering reflections appear in the (001)* reciprocal plane (Figs. 3c and 3d). The extra reflections are different from those observed in the Cr-doped cuprates (18) and therefore suggest a different ordering scheme. HREM along the [001] zone allowed the identification of the type of order and differentiation between long-range order (LRO) and short-range order (SRO). This HREM study also revealed that—on a nanometer scale—the M content is not

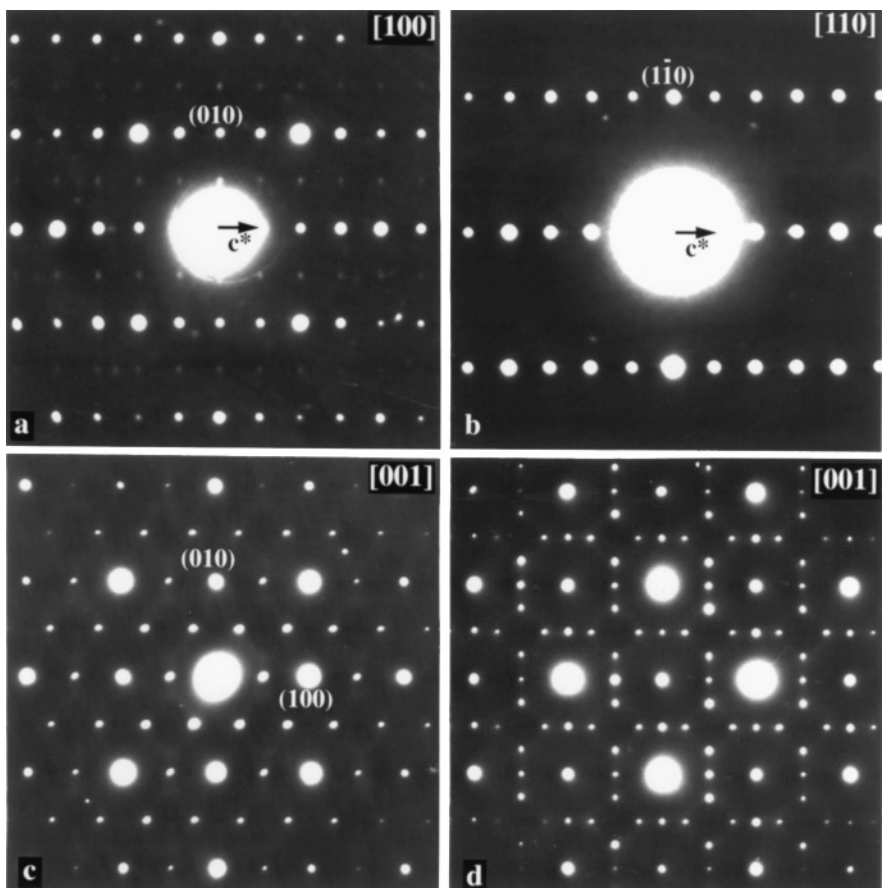

FIG. 3. Electron diffraction patterns of $Tl_{0.8}Ta_{0.2}$ substituted 1201 (a) [100] pattern, exhibiting only weak ordering reflections along [010]*. (b) [110] pattern. (c) [001] pattern from a single orientation variant. (d) [001] pattern including two mutually perpendicular orientation variants.

homogeneously distributed and that LRO areas, SRO areas, or areas without ordering can be detected. HREM along the [100] zone axis indicates that the ordering indeed occurs within the (Tl, M) layer. The ordering depends on the local amount of doping in the Tl layer, i.e., the x value. We will describe the different Tl–M orderings in the following paragraphs.

3.2.1. ($Tl_{1-x}M_xO$) *layers with* $M = Ta$ *or* Nb *and* $0.2 < x < 0.3$. For Ta- and Nb-substituted cuprates extra reflections appear at positions 1/2 0 0, 0 1/2 0, 1/2 1/4 0, and 1/4 1/2 0, i.e., only in the (001)* zone (Figs. 3c and 3d). These reflections clearly belong to two different orientation variants and can be separated by selecting a small enough region (Fig. 3c). The fact that the ordering reflections are sharp and well defined means that the ordered domains are large and well ordered. Often however the ordering reflections are streaked along the $\langle 210 \rangle$* directions, pointing toward the presence of planar defects perpendicular to this direction (see further).

Direct visualization of this ordering is evident from high resolution electron microscopy (HREM) along the [001] direction. An image of a well-ordered region is shown in the left hand part of Fig. 4. The underlying square lattice of 3.8×3.8 Å is clearly visible, but superimposed one observes a superlattice of strong black dots in a lozenge configuration. They define in projection a rectangular superstructure of $4a_{1201} \times 2a_{1201}$, which is outlined in Fig. 4. Along the c axis the 1201 period of 9 Å is maintained and the ordering is only visible in specific patterns such as [100] (see Fig. 3a) or [120]; other patterns such as [110] (Fig. 3b) do not show any ordering reflections. HREM images along [100] indicate that the ordering occurs within the (Tl–M) layer and computer simulation indicate that the dark dots correspond to the Ta atoms within the Tl–O plane. The present contrast only occurs for well-defined thicknesses and defocus values; for most arbitrary values of thickness and defocus, the ordering is hardly visible.

The ordered layer therefore has a composition $(Tl_{0.75}Ta_{0.25-\varepsilon}\square_\varepsilon)O_1$ and the corresponding compound can be described as orthorhombic, point group 2/*mmm*, with approximate lattice parameters $a_0 = 4a_{201} \approx 15.2$ Å, $b_0 = 2a_{1201} \approx 7.6$ Å, and $c_0 = c_{1201} \approx 9.0$ Å.

The schematic ordering between Tl and Ta (or vacancies) for $x = 0.25$ is consistent with the HREM observations of Fig. 4 and is represented in Fig. 5b. In fact, this ordering is easily understood by the different size of the Tl and Ta atoms. Moreover, the introduction of Ta (or vacancies) on the Tl sublattice tends to bring the oxygen atoms closer together around the Ta sites, forming smaller TaO_6 octahedra than the Tl polyhedra. Actually a displacement pattern of the oxygen atoms with respect to the ideal cubic rock

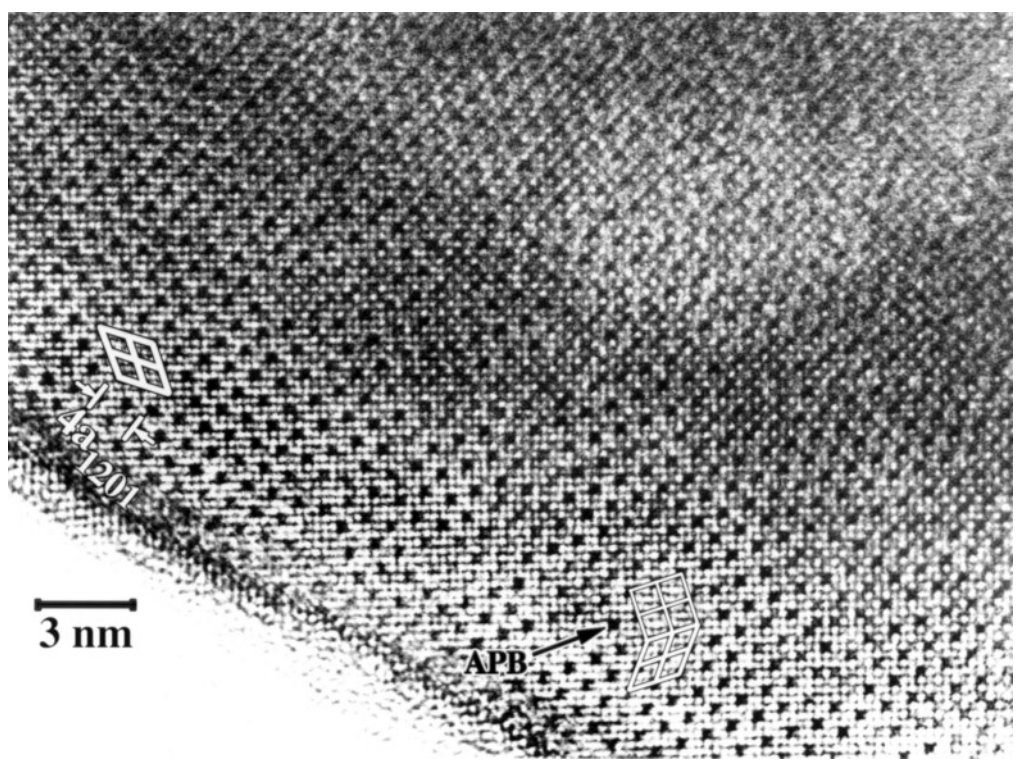

FIG. 4. [001] HREM of $Tl_{1-x}Ta_xSr_2CuO_{5\pm z}$, showing the perfect structure on the left and an translation interfaces at the right.

salt arrangement can be proposed; it is represented in more detail in Fig. 5e and the oxygen shifts are indicated by arrows. In this plane the Ta–O interatomic distances decrease and with the two oxygens located above and below the plane they form a TaO_6 octahedron. As a consequence the Tl surrounding also changes; some oxygens are displaced away from the Tl considered and others are displaced sideways. One can say that the Tl surrounding tends toward tetrahedral or at least toward a "4 + 2" configuration. This is in agreement with the neutron data previously obtained for the 1212 Tl-based cuprates (22).

As evidenced by the diffraction pattern of Figs. 3c and 3d, two different orientation variants can occur, with the long a_0 axis along one of the equivalent a_{1201} axes. As we will see further this ordering very much resembles the oxygen-deficient transition metal oxides with the rocksalt-type structure, such as TiO_x (23), where a Ti–□ ordering takes place, or with the DO_{22}-type ordering in fcc-based alloys (24, 25).

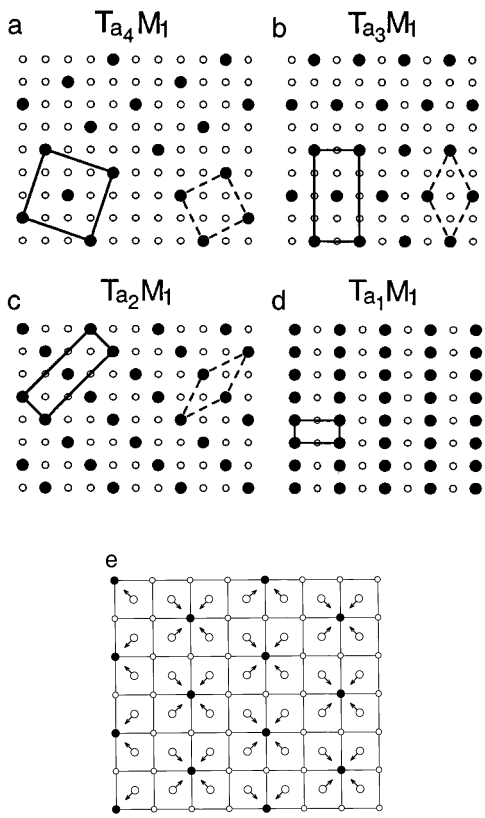

FIG. 5. Two-dimensional schematic configuration of the $(Tl_{1-x}M_x)$ ordering for different x values. (a) $x = 0.20$; (b) $x = 0.25$; (c) $x = 0.33$; (d) $x = 0.50$; (e) detailed configuration, including possible oxygen shifts for $x = 0.25$. Small open circles represent Tl and closed circles are Ta; the larger circles represent oxygen. The arrows show the coordinated displacement of the oxygen atoms, allowing smaller TaO_6 octahedra to be formed. As a consequence Tl atoms tend to adopt a "4 + 2" (pseudo tetrahedral) coordination.

Translational ordering defects are not directly evidenced in the diffraction pattern (apart from a streaking) but they are revealed in the HREM images. They tend to be preferentially situated in the $(210)_{1201}$ plane (or in the related (120) plane); examples are shown in the right hand part of Fig. 4. Across such antiphase boundary (APB) the configuration of the Ta atoms (dark patches in Fig. 4) is no longer triangular, but square. The displacement vector of the nonconservative APB with respect to the orthorhombic unit cell is $\mathbf{R}_0 = 1/4[100]$. Such nonconservative APB alters the local composition, which becomes now $Tl_{0.8}Ta_{0.2}$; a two-dimensional schematic configuration is reproduced in Fig. 5a. The presence of a number of such defects along their preferential $(110)_0$ plane explains the streaking observed in most diffraction patterns, such as Fig. 6a. Actually most crystals show a mixture of both types of ordering on a nanometer scale.

3.2.2. $(Tl_{1-x}Ta_x)O$ layers ($x > 0.3$). For a slightly higher Ta or Nb content—which locally occurs within the same sample—the ordering is different and supplementary reflections appear at positions 1/3 1/3 0 and 2/3 2/3 0 (Fig. 6b). Such an ordering corresponds to a composition $Tl_{2/3}Ta_{1/3}$ and is represented schematically in Fig. 5c. This ordering scheme however does not seem to be very favourable since the ordering reflections are always weak and very diffuse. Actually in the alloy Ni–Mo, where all these ordered phases also appear, the ordering of Ni_2Mo is much more sluggish than the ordering of Ni_3Mo or Ni_4Mo (24).

For x values around 0.5, still another ordered phase does occur; its diffraction pattern and related HREM image is shown in Fig. 7. There is clearly a doubling of the a_{1201} parameter (Fig. 5d). A similar pattern is observed in oxygen-deficient $YBa_2Cu_3O_{7-x}$, where the superstructure is related to an oxygen-vacancy ordering within the CuO_{1-x} plane (26). In the present case the ordering is definitely due to the ordering of Tl and Ta (or Nb); this conclusion not only follows from the local composition determination of EDX, but is also compatible with the intensity of the superstructure reflections. It is remarkable to note that the equivalent phase does not exist in the Ni–Mo alloy, for the simple reason that for the Ni_1Mo_1 composition the fcc lattice is no longer stable (24).

3.2.3. $(Tl_{1-x}W_x)O$ ($0.2 < x < 0.3$). [001] electron diffraction patterns of this compound (Fig. 8, left) show at first glance a completely different aspect; all patterns are alike and show fourfold symmetry and only weak diffuse intensity is present at positions 1/2 1/4 0. In view of the previous observations in the Ta or Nb compounds, this could point toward an ill-defined ordering. The corresponding HREM image (Fig. 9) indeed shows an arrangement of black dots, which at first glance looks disordered, but the Fourier spectrum of this HREM image (see Fig. 11) reveals the

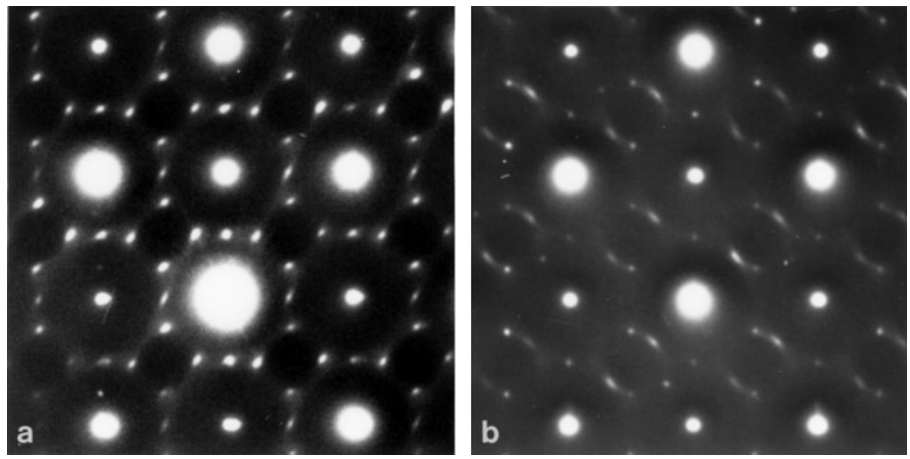

FIG. 6. (a) [001] diffraction pattern of a defective crystal containing a high density of $(210)_{1201}$ and $(120)_{1201}$ planar defects for $0.2 \leq x \leq 0.25$, (b) [001] diffraction pattern of Nb-substituted 1201 for $x \approx 0.33$.

same diffuse intensity as the electron diffraction pattern, indicating the presence of some ordering. Close inspection of the HREM image indeed confirms that the arrangement of black dots mainly consists of triangles (lozenges) and squares, in the same configuration as discussed for the Ta compound. We can process the image, highlight the ordering, and quantify it in the same way as we did for the 1 1/2 0 ordering in alloys (27); the results for the ordered Ta compound and the short-range ordered W compound are summarized in Figs. 10 and 11, respectively. In Fig. 10d one clearly notices the lozenge-shaped units and the antiphase boundaries with the square configuration. The Fourier transform of the processed nd schematized image indicates that no information is lost or altered during the processing. The same processing in applied to the short-range ordered compound (Fig. 11) and now it is clear that although a lot of disorder exists, particular nano-clusters of squares and lozenges preferentially occur. Again the Fourier transform maintains the diffuse intensity at the 1/2 1/4 0 positions. We can quantify the short-range order and determine the short-range order coefficients from such HREM images, the same way as we have done for the Ni–Mo-type alloys (27).

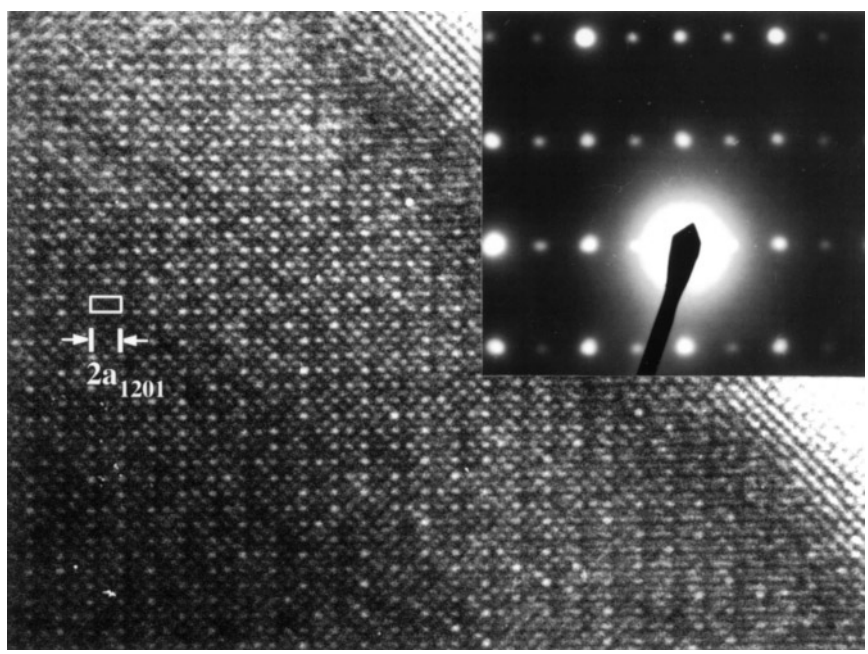

FIG. 7. HREM and electron diffraction pattern (inset) along [001] for a compound with a local composition $Tl_{0.5}Nb_{0.5}$.

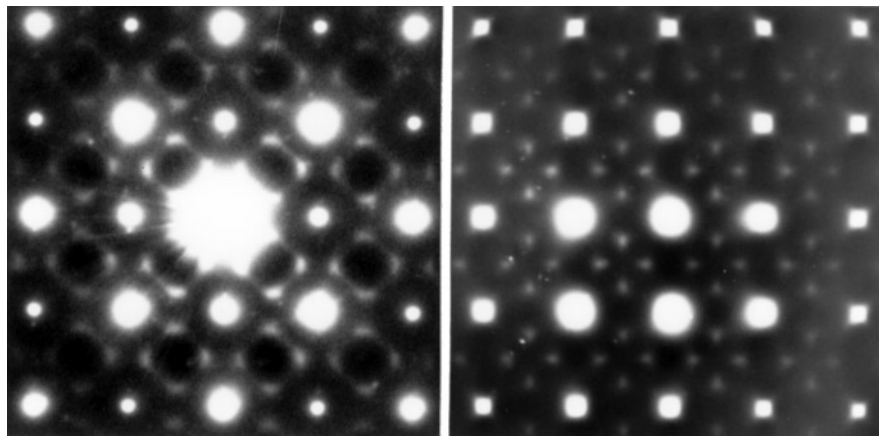

FIG. 8. [001] electron diffraction pattern of $Tl_{1-x}W_xSr_2CuO_{5\pm z}$. (Right) [001] electron diffraction pattern of SRO Ni_4Mo, quenched from high temperature. Note the similarity between both patterns.

[100] HREM images do not reveal any ordering, but because of the similarity with the Ta compound we can safely assume that the ordering takes place within the Tl–W plane.

4. DISCUSSION

The ordered [001] diffraction patterns in these 1201-based compounds show a remarkable similarity with the so-called "1 1/2 0" ordering in fcc-based alloys of the prototype Ni–Mo in the composition range Ni_4Mo–Ni_2Mo (24). Other members of this "1 1/2 0" family, showing similar ordering, are Ni_4W (28), Au_4Cr (29), Au_4Ti (30), Au_4Mn (31), Au_4Fe (32, 33), and Au_4V (32, 34); they all exhibit the D1*a* long-range ordered superstructure and have a unique short-range order state which is such that the short-range order reflections appear at $(1\ 1/2\ 0)_{fcc}$ positions, different from the long-range order positions. Ni–Mo is particular because its phase diagram shows different ordered structures (Ni_4Mo, Ni_3Mo, and Ni_2Mo) which are

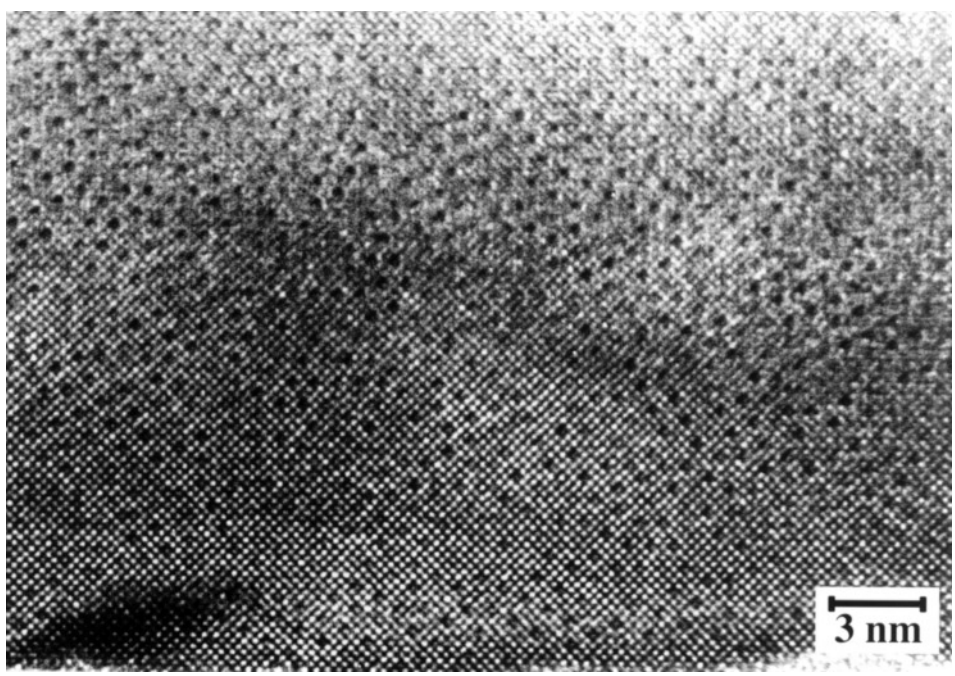

FIG. 9. [001] HREM image of $Tl_{1-x}W_xSr_2CuO_{5\pm z}$.

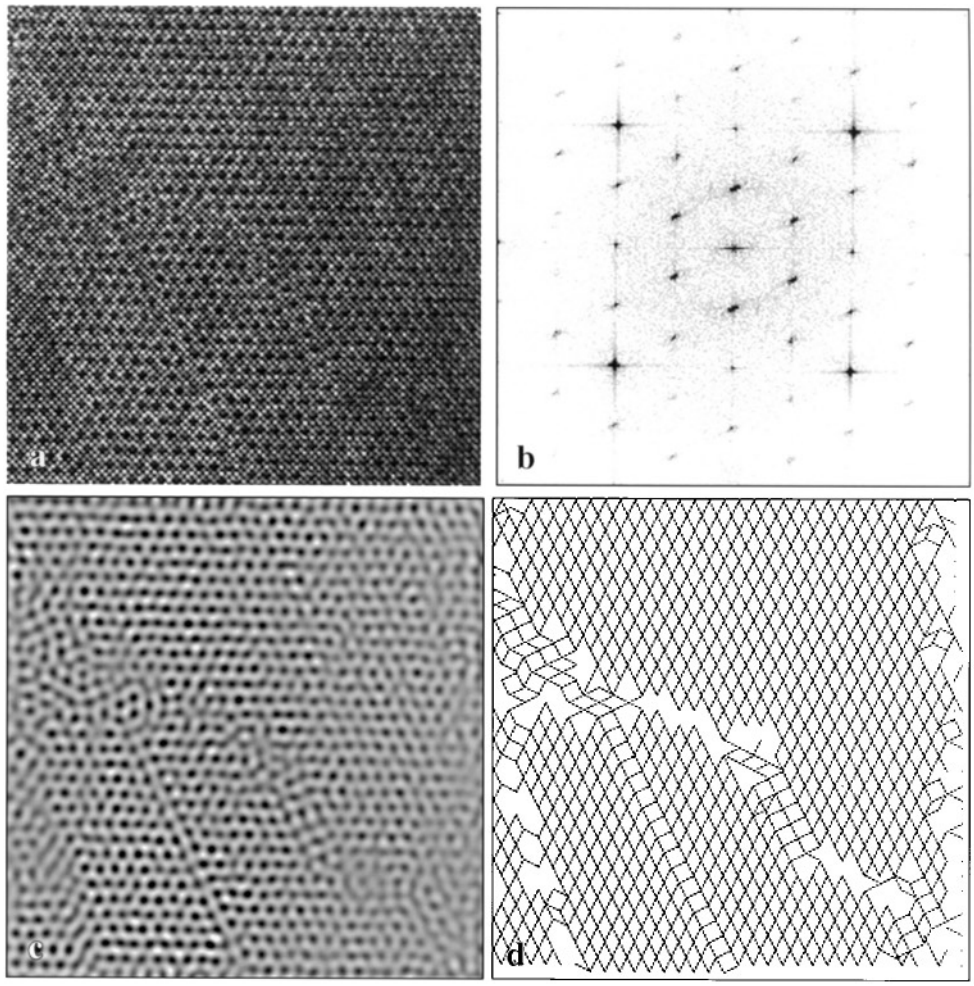

FIG. 10. (a) Original [001] HREM image taken from part of Fig. 3. (b) Fourier transform of 10a. (c) Fourier filtered image. (d) Processed image highlighting the ordering and the defects present.

closely related to each other and which can be derived from each other by introduction of nonconservative antiphase boundaries in the basic DO_{22} compound with a 3–1 composition (24). For about 30 years a controversy has been going on about the real space nature of the short-range order in these compounds; is it better described in function of "concentration waves" (32, 34, 35) or can we associate the short-range order with "microclusters" (36). In a recent paper (27) some of the present authors argued that both models are actually two descriptions of the same physical reality. Indeed the "materialization" of a concentration wave in a discrete medium results in a geometrical pattern that can be considered as a cluster. The main reason for the conflict is associated with the fact that electron microscopy only provides a two-dimensional projected structure of essentially a three-dimensional ordering. This does not create any problem for the LRO state, where one has coherency over long distance with respect to the thickness of the crystal, which is on the order of 10 nm for HREM. For the SRO state or the initial stages of LRO however, when the coherency decreases below the thickness of the sample, the interpretation of the projected image creates severe problems. However, De Meulenaere *et al.* (27) showed that with sufficient care and image processing, the essential information on the ordering is maintained in the image.

The main difference with the present compounds is the dimensionality: the disordered state for the alloys is cubic (fcc), and ordering can occur along the three equivalent cube directions. The 1201 Tl-based compounds are tetragonal; i.e., the c direction is invariably the c_{1201} direction. This strongly reduces the number of orientation variants for the ordered orthorhombic structure (point group $2/mmm$ of order 8); in a cubic matrix (order 48) there are six orientation variants, while in a tetragonal matrix (order 16) there are only two orientation variants left (37). This makes the

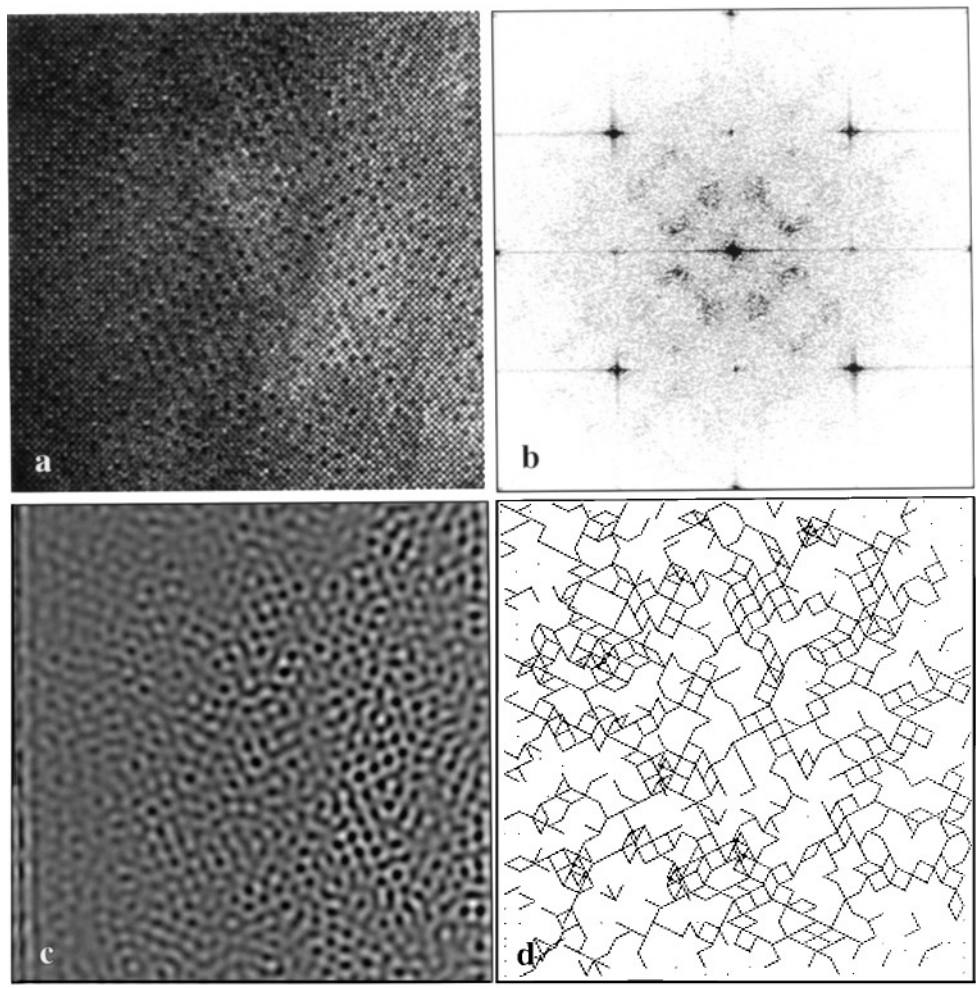

FIG. 11. (a) Original [001] HREM image taken from part of Fig. 8. (b) Fourier transform of 11a. (c) Fourier filtered image. (d) Processed image highlighting the formation of nano-clusters of squares (composition 4–1) and lozenges (composition 3–1).

interpretation in the $(Tl_{1-x}M_x)Sr_2Cu_{1-y}M_yO_5$ system much more straightforward. The results in the $(Tl_{1-x}M_x)Sr_2Cu_{1-y}M_yO_5$ system are totally consistent with the interpretation proposed for the 1 1/2 0 alloys. The "SRO" in the Tl–W compound is clearly an intense mixture of lozenge and square nano-clusters; in the three–dimensional alloys, these correspond to the DO_{22} structure (A_3B composition) and the D1a structure (A_4B composition), respectively.

5. CONCLUSION

New materials with interesting structural properties have been synthesized by introducing Ta, Nb, or W inside the thallium Sr-based 1201 matrix. EDS and XRD show that the actual doping content per unit structural formula ranges from 0.35 for Nb to 0.2 for W. These transition elements occupy Tl and Cu sites. Electron diffraction and HREM show that the distribution of the Tl and M cations within the Tl layer is not random but that ordering takes place.

Although the average cation composition is homogeneous, the grains show different superstructures coherent with the 1201 matrix. These new superstructures correspond to the formation of ordered $(Tl_{1-x}M_xO)$ layers, which have been analyzed by TEM. The two-dimensional ordering on the Tl sublattice is similar to that observed in TiO_x and to the ordering in so-called "1 1/2 0" fcc-based alloys. Because of the two-dimensional character of the cuprates the short-range order can be readily interpreted in terms of a mixture of two different nano-clusters with a different composition.

From EDS, as well as from XRD measurements, the considered materials are homogeneous and can be considered as true new phases. On a nanostructural scale however the composition and the structural arrangement locally vary.

The absence of superconductivity in these materials is easily understood considering the partial substitution of copper by the transition element.

ACKNOWLEDGMENTS

This work is the result of a collaboration within the framework of the HCM program (Contract CHRXCT 940461) of the EEC.

REFERENCES

1. F. Goutenoire, P. Daniel, M. Hervieu, G. Van Tendeloo, C. Michel, A. Maignan, and B. Raveau, *Physica C* **216,** 243 (1993).
2. J. Shimoyama, S. Hahakura, K. Kitazawa, K. Yamajuji, and K. Kishio, *Physica C* **224,** 1 (1994).
3. A. Maignan, M. Hervieu, C. Martin, C. Michel, and B. Raveau, *Physica C* **232,** 15 (1994).
4. G. Van Tendeloo, M. Hervieu, X. F. Zhang, and B. Raveau, *J. Solid State Chem.* **114,** 369 (1995).
5. D. Pelloquin, A. Maignan, S. Malo, C. Michel, M. Hervieu, and B. Raveau, *J. Mater. Chem.* **5,** 701 (1995).
6. C. Michel, M. Hervieu, A. Maignan, D. Pelloquin, V. Badri, and B. Raveau, *Physica C* **241,** 1 (1995).
7. A. Maignan, D. Pelloquin, S. Malo, C. Michel, M. Hervieu, and B. Raveau, *Physica C* **243,** 233 (1995).
8. A. Maignan, D. Pelloquin, M. Hervieu, C. Michel, and B. Raveau, *Physica C* **243,** 214 (1995).
9. J. S. Kim, J. S. Winnea, and H. Steinfink, *J. Less Common Met.* **156,** 347 (1989).
10. A. K. Ganguli and M. A. Subramanian, *J. Solid State Chem.* **93,** 250 (1991).
11. F. Letouzé, C. Martin, A. Maignan, C. Michel, M. Hervieu, and B. Raveau, *Physica C* **254,** 33 (1995).
12. M. H. Pan and M. Greenblatt, *Physica C* **184,** 235 (1991).
13. D. Bourgault, C. Michel, J. Provost, M. Hervieu, and B. Raveau, *J. Solid State Chem.* **26,** 1 (1989).
14. M. H. Pan and M. Greenblatt, *Physica C* **176,** 80 (1991).
15. C. Martin, D. Bourgault, C. Michel, J. Provost, M. Hervieu, and B. Raveau, *Eur. J. Solid State Inorg. Chem.* **26,** 1 (1989).
16. G. H. Kwei, J. B. Shi, and H. C. Ku, *Physica C* **174,** 180 (1991).
17. Z. Z. Sheng, Y. E. Li, Y. Q. Tang, Z. Y. Chen, and D. O. Pederson, *Solid State Commun.* **83,** 205 (1992).
18. C. Martin, F. Letouzé, A. Maignan, R. Seshadri, C. Michel, M. Hervieu, and B. Raveau, *Chem. Mater.* **8,** 865 (1996)
19. H. M. Rietveld, *Acta Crystallogr.* **22,** 61 (1967); *J. Appl. Crystallogr.* **2,** 65 (1969).
20. J. Rodriguez Carvajal, *in* "Collected Abstracts of Powder Diffraction. Meeting Toulouse, July 1990" (J. Galy, Ed.), p. 127. 1990.
21. M. Hervieu, G. Van Tendeloo, C. Michel, D. Pelloquin, and B. Raveau, *Microsc. Microanal., Microstruct.* **7,** 107 (1995).
22. C. Michel, E. Suard, V. Caignaert, C. Martin, A. Maignan, M. Hervieu, and B. Raveau, *Physica C* **178,** 29 (1991).
23. D. Watanabe, O. Terasaki, A. Jostsons, and J. R. Castles, *in* "The Chemistry of Extended Defects in non-Metallic Solids" (Leroy Eyring and M. O'Keefe, Eds.), p. 238. North Holland, Amsterdam, 1970.
24. G. Van Tendeloo, *Mater. Sci. Eng.* **26,** 209 (1976).
25. G. Van Tendeloo, R. De Ridder, and S. Amelinckx, *Phys. Status Solidi* (*a*) **27,** 457 (1975).
26. G. Van Tendeloo, H. W. Zandbergen, and S. Amelinckx, *Solid State Comm.* **63,** 603 (1987).
27. P. De Meulenaere, G. Van Tendeloo, J. Van Landuyt, and D. Van Dyck, *Ultramicroscopy* **60,** 265 (1995).
28. G. Van Tendeloo, N. S. Mishra, and C. Suryanarayana, *J. Mater. Sci.* **11,** 1175 (1976).
29. J. Dutkiewicz and G. Thomas, *Metall. Trans. A* **6,** 1919 (1975).
30. P. Van Heerden, M. P. Shaw, and D. Shechtman, *Phil. Mag. B* **66,** 361 (1992).
31. G. Van Tendeloo, R. De Ridder, and S. Amelinckx, *Phys. Status Solidi* (*a*) **49,** 655 (1978).
32. G. Van Tendeloo, S. Amelinckx, and D. de Fontaine, *Acta Crystallogr. B* **41,** 281 (1985).
33. E. Dartyge, H. Bouchiat, and P. Monod, *Phys. Rev. B* **25,** 6995 (1982).
34. W. M. Stobbs and S. H. Stobbs, *Phil. Mag. B* **53,** 537 (1986).
35. A. G. Khachaturyan, *Phys. Status Solidi* (*b*) **60,** 9 (1973).
36. E. Ruedl, P. Delavignette, and S. Amelinckx, *Phys. Status Solidi* **28,** 305 (1968.
37. G. Van Tendeloo and S. Amelinckx, *Acta Crystallogr. A* **30,** 431 (1974).